Atmospheric Environment 302 (2023) 119755

Contents lists available at ScienceDirect

Atmospheric Environment

journal homepage: www.elsevier.com/locate/atmosenv

VOCs sources and roles in O_3 formation in the central Yangtze River Delta region of China

Zhiqiang Liu [a,b], Kun Hu [c], Kun Zhang [a], Shengnan Zhu [b], Ming Wang [c,**], Li Li [a,*]

[a] School of Environmental and Chemical Engineering, Shanghai University, Shanghai, 200444, China
[b] Jiangsu Changhuan Environment Technology Co., Ltd., Changzhou, 213002, China
[c] Collaborative Innovation Center of Ambient Environment and Equipment Technology, Jiangsu Key Laboratory of Ambient Environment Monitoring and Pollution Control, School of Environmental Science and Engineering, Nanjing University of Information Science & Technology, Nanjing, 210044, China

HIGHLIGHTS

- O_3 formation in Changzhou was in the VOCs-limited regime.
- O_3 formation was most sensitive to xylene and propene at Changzhou.
- Traffic-related emissions was the dominant sources VOCs in Changzhou.
- Reduction ratio of VOCs/NOx should be above 1.6 to curb O_3 pollution in Changzhou.

ARTICLE INFO

Keywords:
Ozone
Observation-based model
Volatile organic compounds
Source apportionment

ABSTRACT

Surface ozone (O_3) pollution has become a prominent air quality problem in the Yangtze River Delta (YRD) region of China in recent years. Since O_3 is non-linearly related to its precursors (volatile organic compounds (VOCs), nitrogen oxides (NO_x)), identifying the characteristics of VOCs is significant for the control of O_3 pollution. In this study, online observation of ambient VOCs from August to October 2018 was conducted at 2 sites in Changzhou, an industrial city located in the central YRD region, to investigate the O_3 pollution characteristics, sources of VOCs, and their roles in O_3 formation. The average concentration of VOCs in Changzhou during the observational period was 39.52 ± 23.14 ppb. Alkanes, oxygenated VOCs (OVOCs), and halocarbons were the main contributors to the total VOCs concentration, with the average relative contributions of 39.4%, 23.1%, and 16.1%, respectively. An observation-based model (OBM) was used to investigate the sensitivity of O_3 formation to VOCs and NO_x. Results of relative incremental reactivity (RIR) of individual VOC and empirical kinetics modeling approach (EKMA) showed that the O_3 formation in Changzhou was within the VOCs-limited regime. Anthropogenic VOCs with the largest RIR values were xylenes and propene, respectively. The positive matrix factorization (PMF) model was applied to quantitatively identify the sources of VOCs. Six factors were resolved, including vehicle exhaust, gasoline evaporation, paint and solvent usage, electronic manufacturing, petrochemical industry, and biogenic source & secondary formation. The average relative contribution of traffic-related emissions to the total VOCs mass concentration was about 49.5%, followed by electronic manufacturing (22.9%), paint and solvent usage (14.7%), and petrochemical industry (7.1%). The average relative contributions of individual sources for xylenes and propene were further compared. Xylenes were mainly emitted from paint and solvent usage (60%), electronic manufacturing (17%), and vehicle exhaust (16%). Petrochemical industry (67%) and vehicle exhaust (30%) were the major sources of propene. Therefore, VOCs from industrial emissions and traffic-related emissions should be given priority for the control of O_3 pollution in the central YRD region.

* Corresponding author.
** Corresponding author.
E-mail addresses: wangming@nuist.edu.cn (M. Wang), lily@shu.edu.cn (L. Li).

https://doi.org/10.1016/j.atmosenv.2023.119755
Received 21 October 2022; Received in revised form 30 January 2023; Accepted 27 March 2023
Available online 28 March 2023
1352-2310/© 2023 Elsevier Ltd. All rights reserved.

1. Introduction

Surface O_3 is mainly from the photochemical oxidation of VOCs and NO_x (Tan et al., 2018). Understanding the roles of VOCs and NO_x in O_3 formation is the basis for formulating effective O_3 control measures. Therefore, it is necessary to determine the nonlinear relationship between O_3–VOCs-NO_x. The OBM is a commonly used method for O_3 sensitivity analysis and is an important supplement to the air quality model which investigates O_3–VOCs-NO_x relationship based on emissions inventory. Some O_3–VOCs-NO_x sensitivity studies using the OBM model have been carried out in the YRD region (Zhang et al., 2021, 2022). Results show that the main controlling factor of O_3 formation varied in different cities. The formation of O_3 in the urban area of Shanghai was in the VOCs-limited regime (*i.e.* reduction of VOCs will decrease the O_3 concentration, and reduction of NO_x will have little impact on O_3 or even increase O_3 concentration), while O_3 formation in the suburbs without obvious local sources tend to be in the transition regime (*i.e.* the reduction of VOCs or NO_x will both reduce the O_3 concentration) (Lin et al., 2020). O_3 formation in the urban area of Hangzhou is also in the VOCs-limited regime (Zhang et al., 2020). Different from Shanghai and Hangzhou, the O_3 formation in the urban area of Nanjing is in the transition regime (Wang et al., 2020a), while O_3 formation in the industrial area is mainly controlled by VOCs (Fan et al., 2021).

Compared to NO_x, which is mainly from combustion processes, VOCs sources are more complex. VOCs can be directly emitted from anthropogenic sources and biogenic sources, and can be produced by photochemical oxidation (Tan et al., 2018; Whalley et al., 2021). This would cause challenges for understanding VOCs sources and formulating O_3 control measures. The positive matrix factorization (PMF) model is widely used to analyze VOCs sources based on observations (Zhang et al., 2021; Zhao et al., 2020). For example, the PMF-resolved results suggest that the ambient VOCs in Shanghai from May 20, 2017 to May 30, 2017 are mainly emitted from traffic-related emissions (48%) (Liu et al., 2019), which is higher than that in Nanjing for the whole year of 2016 (37%) (Wang et al., 2020b) and Hangzhou from August 24, 2016 to September 6, 2016 (13.8%) (Zhang et al., 2020). Industrial emissions contributed 61% to the concentration of VOCs in Nanjing, which was higher than those in Shanghai (23%) and Hangzhou (14%).

Changzhou is one of the cities with the most serious O_3 pollution in the YRD region. The daily maximum 8-h averages (MDA8) O_3 in Changzhou in 2020 was 167 μg/m^3, higher than that in Shanghai (152 μg/m^3) (https://sthj.sh.gov.cn/, last access: 2021), Hangzhou (151 μg/m^3) (http://epb.hangzhou.gov.cn/, last access: 2021), Huzhou (160 μg/m^3) (http://hbj.huzhou.gov.cn/, last access: 2021), Zhenjiang (164 μg/m^3) (http://sthj.zhenjiang.gov.cn/, last access: 2021), and Hefei (144 μg/m^3) (https://sthjj.hefei.gov.cn/, last access: 2021), lower than Najing (168 μg/m^3) (http://hbj.nanjing.gov.cn/, last access: 2021), and Wuxi (171 μg/m^3) (http://bee.wuxi.gov.cn/, last access: 2021). An emission inventory study shows that the VOCs from anthropogenic emission in Changzhou in 2015 has reached 11.5 × 10^4 t/year, with the largest relative contribution from the manufacturing-related industry (72%) (Xia et al., 2018). In this study, the online observation of VOCs, O_3, and NO_x were conducted in Changzhou for about 2 months in the summer and autumn of 2018. After analyzing VOCs concentration characteristics, O_3–VOCs-NO_x sensitivity was then investigated using the OBM model and VOCs sources were quantitatively identified using the PMF model. These findings can provide a scientific basis for the prevention and control of ambient VOCs and O_3 pollution in the central YRD region.

2. Methodology

2.1. Observations of VOCs and other trace gases

Online observations of ambient VOCs and other trace gases (e.g., NO_x, O_3, CO) were conducted from August 24 to October 11, 2018, and the time resolution is 1 h. Fig. 1 shows the geographical locations of 2 sites, which were named as S1 site (119.93°N, 31.91°E) and the S2 site (119.99° N, 31.81° E), respectively. The S1 site was mainly surrounded by residential areas, but close to arterial roads (nearly 1–2 km). The S2 site was located in a typical central urban area, mainly surrounded by residential areas and commercial districts. These two sites were selected to compare the O_3 formation mechanisms in urban and suburban areas.

In this study, ninety-nine VOC species, including 28 alkanes, 11 alkenes, acetylene, 17 aromatics, 33 halocarbons, 7 OVOCs, and 2 others were detected by an online cryogen-free automatic gas chromatograph system. The system contains two channels. In one channel, C2–C5 hydrocarbons were separated and detected by a flame ionization detector (FID). In the other channel, halocarbons, OVOCs, and C6–C12 hydrocarbons were separated and detected by a mass spectrometry detector (MSD). More detailed analytical methods, parameter settings, and quality assurance/quality control (QA/QC) procedures of this system have been described by Wang et al. (2014). The method detection limits (MDL) of this system ranged from 0.002 ppbv to 0.046 ppbv. The determination coefficients (R^2) of the calibration curves for the target VOC species were all greater than 0.999. In addition, online observations of O_3, NO, and NO_2 were measured by the UV photometric O_3 analyzer (API, Model 400E) and the chemiluminescence NO–NO_2-NO_x analyzer (API, Model 200E), respectively.

2.2. Models

2.2.1. OBM model

In this study, the relationship between O_3 formation and its precursors (VOCs, NO_x, and CO) was analyzed by a 0-dimension box model developed by Cardelino and Chameides (1995). Apart from photochemical production, subsidence of ozone from the aloft residual layer may also contribute to the increase in the morning. However, the 0-dimensional model did not consider the vertical transport of O_3, which will cause some uncertainty to the results. But if we mainly focus on the near surface photochemistry, the OBM can provide some insights into the O_3 formation. The drawing method of EKMA curve is as follows: 20*20 scenarios are set, and the minimum is reduced to 0 and the maximum is increased to 1 with 5% interval of their average value (Lu et al., 2022). The RIR of each precursor is calculated by the following equation:

$$RIR(X) = \frac{\left(P_{O_3-NO}(X) - P_{O_3-NO}(X-\Delta X)\right)/P_{O_3-NO}(X)}{\Delta S(X)/S(X)} \quad (1)$$

where P_{O3-NO} is the net production of O_3, including the consumption of reaction with NO. S(X) represents the source function for a specific precursor X. ΔX represents the change of X concentration caused by the change of $S(X)$ (*i.e.* $\Delta S(X)$). In this study, the time interval between 07:00–19:00 of each day was chosen for the simulation of O_3 formation, and the hourly average values of VOCs, NO, NO_2, O_3, CO, and temperature were used as inputs. The ratio of $\Delta S(X)/S(X)$ was set as 10% for the RIR calculation (Lu et al., 2010; Wang et al., 2020a). And there was a sensitivity analysis performed for the RIR calculation while the ratio of $\Delta S(X)/S(X)$ was set as 5%, 10%, 15%, and 20%. As shown in Fig. S1, NO_x was most affected by changes in the ratio of $\Delta S(X)/S(X)$, followed by AHC, while NHC and CO hardly change with changes in the ratio of $\Delta S(X)/S(X)$. S1 in SI showed more details about the sensitivity analysis.

2.2.2. PMF model

The PMF model (Version 5.0) developed by the U.S. Environmental Protection Agency (EPA) was used for VOCs source apportionment. The detailed descriptions of the PMF model can be found in its User's Manual (EPA, 2014). In general, PMF was a multivariate factor analytical tool, which decomposes the measurement data into the source profiles matrix and the source contributions matrix. Species selection for PMF is generally based on the following principles: (1) Select VOCs species that

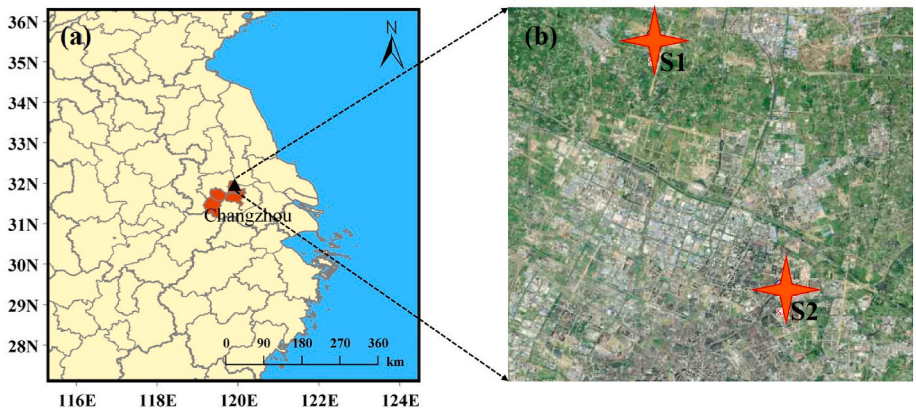

Fig. 1. Locations of VOCs online measurement sites (S1 and S2) in Changzhou.

can indicate a particular source of pollution (e.g., propane is a tracer for LPG sources); (2) These VOC species were mainly selected based on their higher ambient concentration levels, indications for sources, and signal versus noise (S/N) values greater than 5 (i.e. S/N > 5). Twenty-six VOC species were input into the PMF model for VOCs source apportionment, including 10 alkanes, 3 alkenes, acetylene, 6 aromatics, 3 halocarbons, and 3 OVOCs (Fig. 6). The sum of the 26 VOCs concentration accounts for 80.4% of the VOCs concentration, indicating that these 26 VOCs can reflect VOCs main situation. As shown in Fig. S2, the photochemical reaction was not significant during the observation period. Therefore, we did not perform photochemical reaction correction for VOCs to calculate its initial concentration, which would bring some uncertainty to the PMF results. We described this part in detail in S2 of SI. Furthermore, when determining the factor numbers of PMF resolution, 4 to 10 factors were tested. According to the change of Q_{robust}, when the number of factors increased from 5 to 6, the Q_{robust} decreased significantly. When the number of factors increases from 6 to 7, the decrease of Q_{robust} is not obvious. When the factor numbers were set more than 6, one of the resolved factors would be decomposed into multiple factors that could not be explained by a single source. Therefore, the final number of factors was set as 6.

3. Results and discussion

3.1. Characteristics of VOCs, O_3, and NO_x

Fig. 2 compares the average concentrations of VOCs, O_3, and NO_x at 2 sites during the online observation. Overall, the average concentrations of ambient O_3, NO_x, and VOCs at S1 and S2 are relatively close. The average concentrations of O_3 and NO_x at the S1 site were 77.0 ± 50.1 μg/m^3 and 40.1 ± 24.9 μg/m^3, respectively, which were slightly lower than the average concentration of O_3 (83.2 ± 48.7 μg/m^3) and NO_x (43.4 ± 19.5 μg/m^3) at the S2 site. The average concentration of VOCs at the S1 site was 41.2 ± 25.2 ppbv, which was slightly higher than that for the S2 site (37.8 ± 21.1 ppbv).

From the perspective of chemical compositions of VOCs, the relative contributions of 7 VOC categories at these 2 sites are also similar. Alkanes were the largest contributor to the total VOCs concentration, with the relative contributions ranging from 42.9% to 44.7%, followed by OVOCs (16.9%–17.0%), halocarbons (13.3%–15.7%), and aromatics (11.5%–15.2%). The relative contributions of alkenes and acetylene are less than 10%. For individual VOC species, the top three abundant VOC species were propane, acetone, and ethane, with average concentrations in the ranges of 4.55 ppbv–4.65 ppbv, 4.09 ppbv–5.00 ppbv, and 2.30 ppbv–2.54 ppbv, respectively. In addition, the sum of relative contributions of these three species contributes 23.0%–32.2% of the total VOCs concentrations.

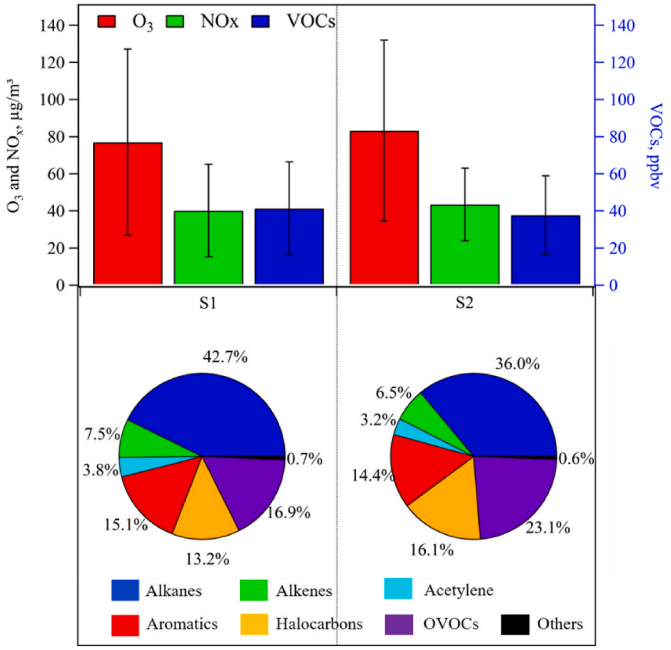

Fig. 2. The average concentration levels of O_3, NO_x, and VOCs (top) and relative contributions of 7 VOCs categories to total VOCs concentrations at the S1 (left-bottom) and S2 (right-bottom) sites during the online observation.

3.2. Diurnal variations of VOCs, O_3, and NO_x

Fig. 3(a–c) shows the average diurnal variations of concentrations for O_3, NO_x, and VOCs at 2 sites during the online observation period. Ambient O_3 concentrations show lower values in the morning and evening, then gradually increase after sunrise and reach the peak value at about 15:00 and then decrease gradually. In contrast with O_3, the average diurnal variations of NO_x and VOCs concentrations both show a "U-shaped" pattern. Their concentrations are higher in the morning and evening and exhibit peaks nearby 7:00–8:00, which are consistent with the traffic rush time in the morning, implying the possible influence of traffic-related emissions. The lowest concentrations of NO_x and VOCs occurred at 13:00–14:00, which may be due to the increase in boundary layer height, the faster turbulent mixing processes, and the rapid consumption of VOCs due to strong photochemical reactions at noon.

Fig. 3(d–j) shows the diurnal variations of alkanes, alkenes, acetylene, aromatics, halocarbons, and OVOCs. The concentrations of alkanes, alkenes, acetylene, and aromatics all show a U-shaped diurnal variation pattern, with higher concentrations in the morning and

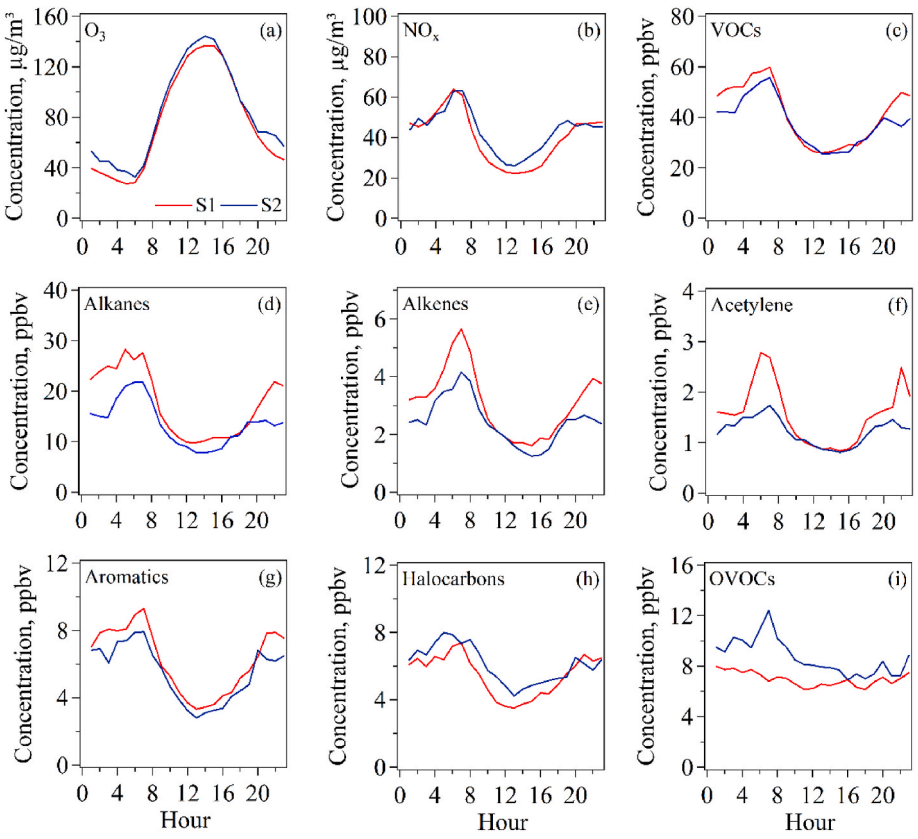

Fig. 3. Average diurnal variation patterns for concentrations of (a) O_3, (b) NO_x, (c) VOCs, (d) Alkanes, (e) Alkenes, (f) Acetylene, (g) Aromatics, (h) Halocarbons, and (i) OVOCs. Red and blue lines represent the S1 and S2 sites, respectively.

evening, and lower values during 13:00–14:00. Although halocarbons show a similar diurnal variation pattern with nonmethane hydrocarbons (NMHCs), their variation range is lower than those for NMHCs, which may be related to its relatively weak chemical reactivity. Different from other VOC categories, average concentrations of OVOCs during each hour maintain a stable level, indicating the possible influence of secondary formation besides primary emission. It should be noted that the concentrations of alkanes, alkenes, acetylene and aromatics at S1 were

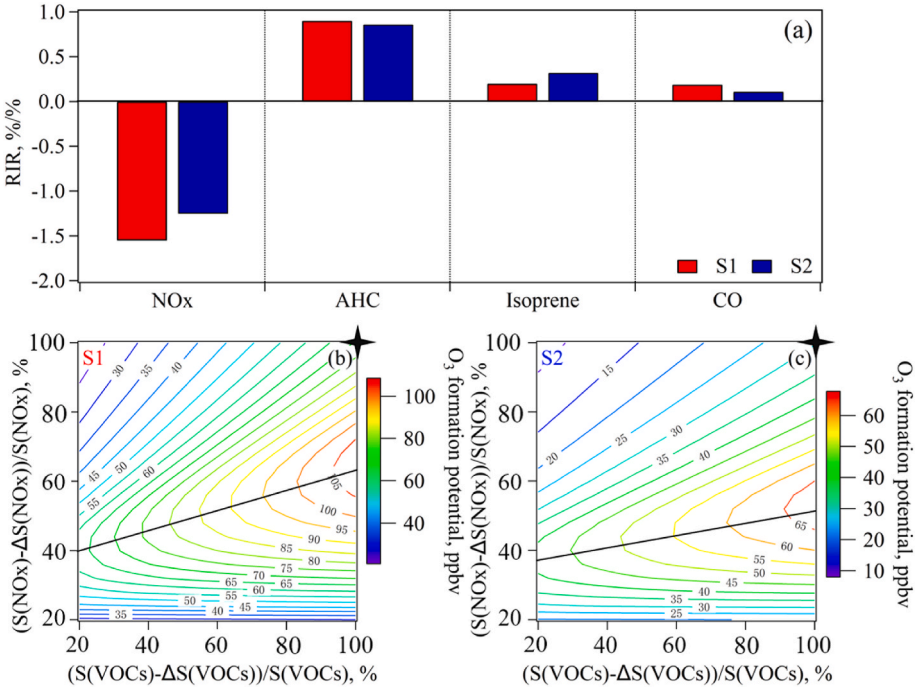

Fig. 4. (a) The average RIR values for NO_X, NHC, AHC, and CO and (b–c) the EKMA curves at 2 sites.

higher than that at S2. According to the wind rose plots of each VOCs group, relatively higher level of alkanes, alkenes, acetylene and aromatics were concentrated when wind speed was less than 1 m/s, suggesting that the local emissions of alkanes, alkene, acetylene and aromatics were stronger at S1 than that at S2 (Figs. S3–5). Previous studies have shown that vehicles emit OVOCs (Liu et al., 2009). Geographically, S2 is closer to the road than S1, and is located at a crossroads. Therefore, S2 is more susceptible to the morning rush hour traffic.

3.3. Roles of VOCs in O_3 formation

3.3.1. O_3 sensitivity to VOCs and NO_x

In this study, online measurements of O_3 and its precursors on O_3 pollution days (*i.e.*, MDA8 O_3 greater than 160 μg/m^3) were chosen to further investigate the sensitivity of O_3 formation to its precursors. There are 18 d and 16 d selected for the S1 and S2 sites, respectively. Fig. 4 (a) shows the average values of RIR for O_3 precursors, including NO_x, anthropogenic NMHCs (AHC), isoprene, and CO at 2 sites. The RIR values of NO_x at 2 sites were both negative, with values of −1.25%/% and −1.59%/%, respectively, indicating that a 10% reduction of NO_x will increase O_3 concentrations by 12.5% and 15.9%, respectively. In contrast with NO_x, the RIR values of AHC, isoprene, and CO are all positive, indicating that a 10% reduction of AHC, isoprene, and CO all result in the decrease of O_3 concentrations. The RIR values of isoprene and CO range from 0.13%/%-0.32%/% and 0.11%/%-0.24%/% respectively, which are significantly lower than that of AHC (0.86%/%-0.94%/%). This indicates that anthropogenic VOCs play a more important role in O_3 formation than isoprene and CO, and therefore reducing anthropogenic VOCs is the most efficient approach to controlling O_3 pollution in the central YRD region.

Fig. 4(b–c) shows the contour plots of O_3 formation potential as a function of the reduction of anthropogenic VOCs (S(VOCs)) and NO_x (S(NO_x)) at 2 sites (*i.e.* EKMA curve). The EKMA curve can be divided into upper-left and lower-right parts according to the ridgeline (black line). The S(VOCs) and S(NO_x) data points in the upper-left part indicating that the O_3 formation is in the VOCs-limited regime, while the data point in the lower-right part indicates that the O_3 formation is in the NO_x-limited regime. The data point near the ridgeline indicates that the O_3 formation is both controlled by anthropogenic VOCs and NO_x (*i.e.* in the transition regime). The O_3–VOCs-NO_x sensitivities at these 2 sites are both in the VOCs-limited regime. This finding is consistent with that obtained from the RIR values. The O_3–VOCs-NO_x sensitivity results in this study are similar to results obtained in most urban areas of the YRD region, the Pearl River Delta (PRD) region (He et al., 2019), and the North China Plain (NCP) region (Sun et al., 2021). This means that reducing VOCs is still an efficient way for the short-term control of O_3.

3.3.2. Identification of key anthropogenic VOCs in O_3 formation

In order to identify the key anthropogenic VOC species in O_3 formation, the RIR values of individual VOC species were also calculated using the OBM. The RIR values of anthropogenic VOC species range from 0.001%/% to 0.267%/%. Fig. 5 shows the anthropogenic VOC species with the top 10 largest RIR values at 2 sites. m,p-Xylene shows the largest RIR value both at the S1 and S2 sites, with values of 0.247%/% and 0.267%/% respectively, followed by o-xylene (0.097%/% and 0.090%/%) and propene (0.080%/%-0.090%/%). The sum of RIR values for xylenes (m,p-xylene and o-xylene) and propene accounted for 48.6% and 50.0% of RIR values in the total anthropogenic VOC species at the S1 and S2 sites, respectively. Therefore, xylenes should be given priority for the control of O_3 pollution in the central YRD region.

3.4. Source apportionments of VOCs using the PMF model

3.4.1. Identification of PMF-resolved factors

Fig. 6 shows the chemical profiles of individual VOCs source resolved by the PMF model in Changzhou during the online observation period. Factor 1 shows high relative contributions to the concentration of C4–C6 alkanes, C2–C3 alkenes, acetylene, benzene, MTBE, *etc.*, with values of 52.6%–92.6%. These VOC species are mainly emitted from vehicle exhaust (Man et al., 2020), so factor 1 is identified as vehicle exhaust. Factor 2 is characterized by high abundances of i-pentane and n-pentane, with mass percentages of 39.1% and 40.6%, respectively. Previous studies reported that i-pentane and n-pentane are the main components of gasoline (Song et al., 2020), so factor 2 is identified as gasoline evaporation. The relative contributions of factor 3 to the concentration of aromatics were ranging from 39.2% to 64.1%. Aromatics are the important components widely used in paint and solvent coating (Mo et al., 2021), so factor 3 is identified as paint and solvent usage#-aromatics. Factor 4 shows high relative contributions to the concentration of halocarbons (42.5%–77.3%) and toluene (46.8%), respectively. Electronic manufacturing is an important industry in Changzhou and a lot of halocarbons and toluene are used for the surface coating of electronics (Lv et al., 2021), so factor 4 is identified as electronic manufacturing#-halocarbons. The major VOC species of factor 5 were ethene and propene. The relative contributions of this factor to ethene and propene were 49.5% and 68.3%, respectively. Alkenes are the key raw materials and products of the petrochemical industry (Mo et al., 2015), so factor 5 is identified as petrochemical industry#-ethene & propene. The relative contributions of factor 6 to concentrations of isoprene, acrolein, and acetone to factor 6 are 86.9%, 33.8%, and 32.7%, respectively. Isoprene is an important tracer to indicate biogenic emissions (Dorter et al., 2020). OVOCs are the intermediate products from ambient photochemical oxidation reactions (Chen et al., 2014), so factor 6 is identified as biogenic emission & secondary formation.

3.4.2. Diurnal variation of VOCs sources resolved by the PMF model

Fig. 7 shows the average diurnal variations of the total VOCs mass concentrations from each factor. VOCs concentrations from anthropogenic sources (*i.e.* vehicle exhaust, gasoline evaporation, paint and

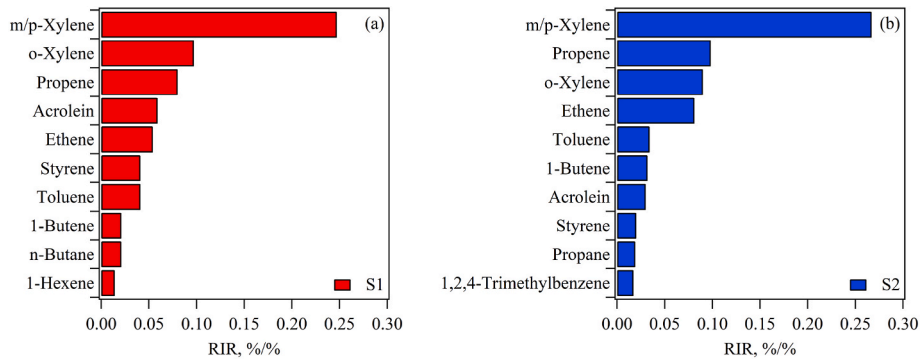

Fig. 5. Anthropogenic VOC species with top 10 RIR values at 2 sites.

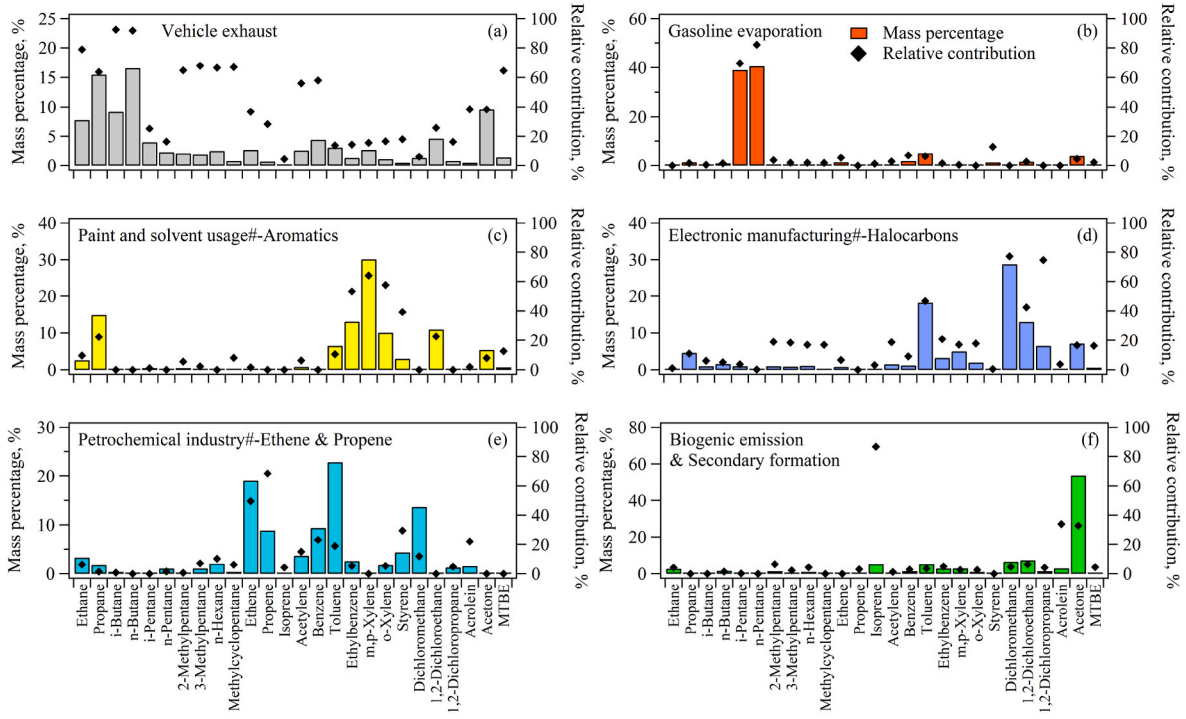

Fig. 6. The chemical profiles of VOCs in 6 factors and resolved by the PMF model.

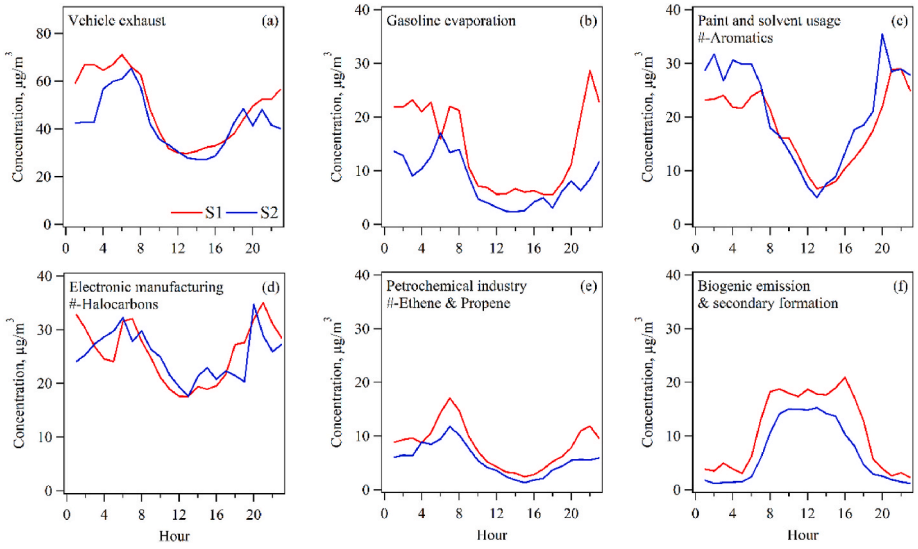

Fig. 7. Average diurnal variation patterns of total VOCs mass contributions from (a) vehicle exhaust, (b) gasoline evaporation, (c) paint and solvent usage#-aromatics, (d) electronic manufacturing#-halocarbons, (e) petrochemical industry#-ethene & propene, and (f) biogenic source & secondary formation. Red and blue lines represent the S1 and S2 sites, respectively.

solvent usage#-aromatics, electronic manufacturing#-halocarbons, and petrochemical industry#-ethene & propene) all show a significant "U-shaped" diurnal variation pattern at 2 sites., with high values during 7:00–8:00 in the morning and the lowest values around 13:00 at noon (Fig. 7a–e). In contrast with anthropogenic sources, VOCs concentration from biogenic emission & secondary formation shows a diurnal variation with a single peak (Fig. 7f). In this pattern, VOCs concentrations are lower in the morning and evening but higher at 09:00–16:00 (about 15 $\mu g/m^3$-20 $\mu g/m^3$). This may be due to the strong solar radiation at noon enhancing the emissions from vegetation and the strong photochemical formation of OVOCs. It is noteworthy that S2 has higher OVOCs than S1, contrary to other VOC species. OVOCs have both primary and secondary sources. According to the results of PMF model, the VOCs concentration contributed by paint and solvent usage#-aromatics at S1 and S2 were 18.2 $\mu g/m^3$ and 20.9 $\mu g/m^3$, which indicated that the OVOCs of site S2 from the primary emission of solvent was higher than site S1. The concentration of ozone at S1 and S2 were 76.6 $\mu g/m^3$ and 83.2 $\mu g/m^3$. It indicated that the photochemical oxidation at S2 is stronger than S1, which resulted in higher OVOCs due to secondary generation at S2 than S1. In conclusion, primary emission and secondary generation lead to higher OVOCs at S2 than S1.

3.4.3. Relative contributions of individual sources for VOCs, xylenes, and propene

Fig. 8(a–b) shows the relative contribution of individual sources to total VOCs mass concentrations at the S1 and S2 sites. Overall, the relative contributions of individual sources at S1 and S2 sites are similar. Traffic-related emissions and industrial emissions are the main sources of VOCs. Vehicle exhaust (38.8%) is the main anthropogenic source of VOCs at the S1 site, followed by electronic manufacturing#-halocarbons (20.4%), paint and solvent usage#-aromatics (14.4%), gasoline evaporation (11.1%), and petrochemical industry#-ethene & propene (6.4%). At the S2 site, vehicle exhaust (39.1%) shows the dominant contribution to VOCs, followed by electronic manufacturing#-halocarbons (23.0%), paint and solvent usage#-aromatics (18.9%), paint and solvent usage#-aromatics (7.3%), and petrochemical industry#-ethene & propene (5.1%). The number of vehicles in Changzhou reached 1.5×10^6 in 2020 (http://tjj.changzhou.gov.cn/html/tjj/2021/OEJCMFCP_1025/26977.html), and thus vehicle exhaust has become an important source of ambient VOCs. Changzhou is also a city with developed industries. The chemical industry, electronic manufacturing, automobile coating, iron and steel industry, *etc.* are key industries in Changzhou, which could have important influences on ambient VOCs.

Based on the results of OBM, xylenes and propene are the key anthropogenic VOC species for O_3 formation. The relative contributions of individual sources to these two VOC species at the 2 sites were further investigated. Industrial emissions were the dominant contributor for xylenes at 2 sites, with relative contributions of paint and solvent usage#-aromatics (60%), electronic manufacturing#-halocarbons (17%), and vehicle exhaust (16%), respectively (Fig. 8c–d). Different from xylenes, the petrochemical industry#-ethene & propene and vehicle exhaust are the major sources of propene (Fig. 8e–f). The relative contribution of petrochemical industry#-ethene & propene to propene at the S1 and S2 sites have reached 72.9% and 61.2% respectively, then followed by vehicle exhaust (23.1% and 38.3%). These results show that paint and solvent usage, the petrochemical industry, vehicle exhaust, and electronic manufacturing should be given a priority for controlling VOCs and O_3 in Changzhou.

3.4.4. Comparison between the PMF results and emission inventory

In this study, vehicle exhaust is the main source of Changzhou VOCs, and the relative contribution rate at S1 and S2 are 38.8% and 39.1%, respectively, which are higher than the result (14.1%) in the list established by Xia et al. (2018). This suggests that the contribution of vehicle exhaust may be underestimated in the inventory. While paint and solvent usage in this study contributed 14.4% and 18.9% to VOCs at S1 and S2, respectively, which were lower than the inventory (45.1%) compiled by Xia et al. (2018). Temporal and spatial distribution, emission intensity, source structure and other factors will affect the uncertainty of VOCs emission inventory. The contribution of vehicle exhaust and paint and solvent usage to VOCs is significantly different in the receptor model and emission inventory, which means that there are great uncertainties in these types of sources. It is need to be paid attention to in the future studies of receptor model and emission inventory to improve the accuracy of contribution assessment of these sources.

4. Control strategies for ozone pollution episodes

The above analysis illustrates the sources of O_3 precursor and the sensitivities of O_3 formation. However, it is unclear how to formulate the policies to better diminish O_3 pollution. Hence, multi-scenario analyses with different reduction ratios of NO_x and VOCs were conducted to explore the non-linear response of O_3 formation under different emission reduction policies. As shown in Fig. 9, the horizontal and vertical axis represent the reduction percentages of NO_x emission and the O_3 formation rates ($P(O_3)$), respectively, and each curve in Fig. 9 represents different reduction percentages of VOCs. It should be noted that $P(O_3)$ increased as the reduction ratio of NO_x increased from 0% to 40% at S1 or from 0% to 60% at S2, regardless of the reduction of anthropogenic hydrocarbons (AHC), while $P(O_3)$ decreased when NO_x was reduced by

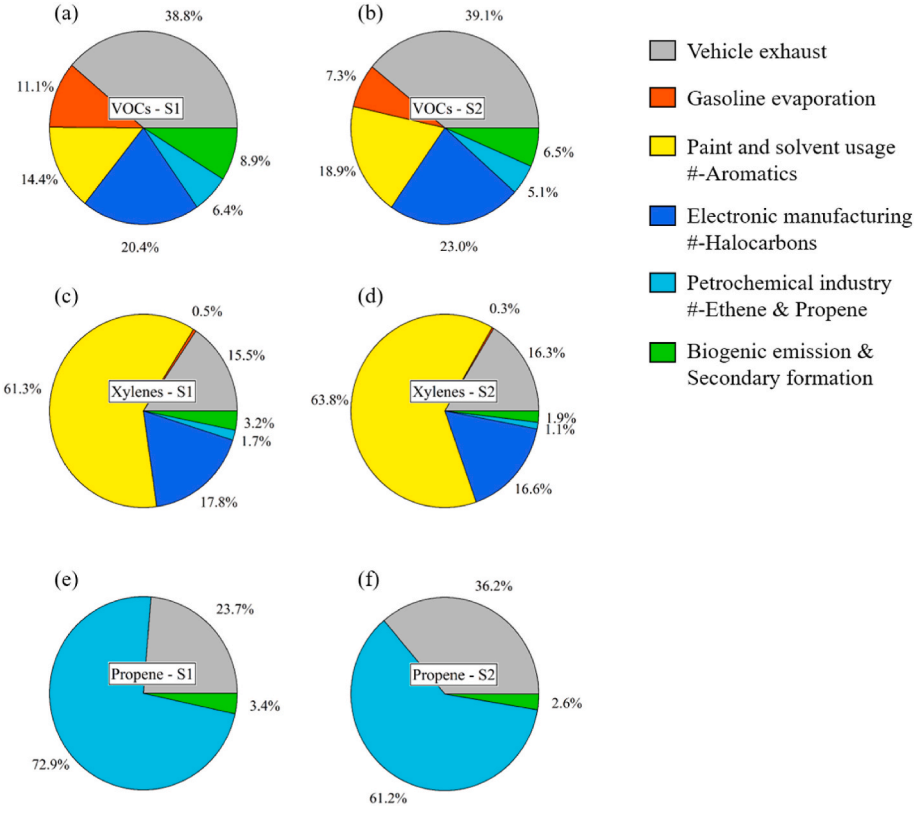

Fig. 8. Source apportionments of (a–b) VOCs, (c–d) xylenes, and (e–f) propene at 2 sites.

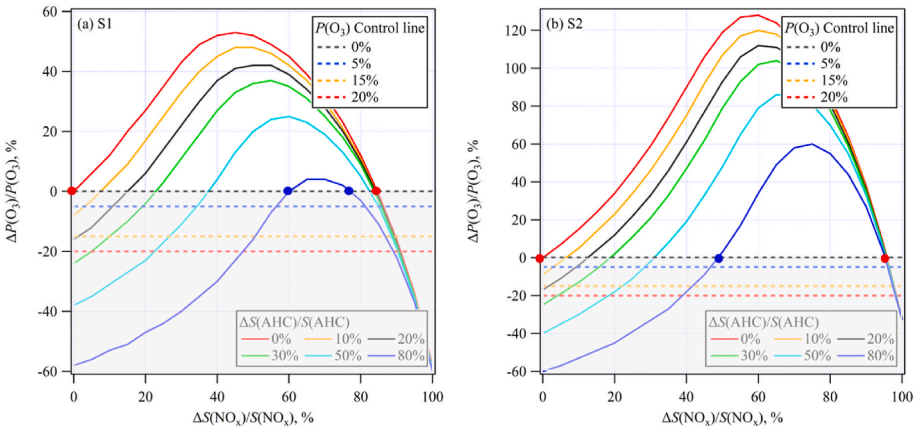

Fig. 9. Reduction of O_3 production rate as a function of reduction percentages of NO_x and VOCs.

>40% and 60% at S1 and S2, respectively. However, an efficient control strategy would lead to the decrease of $P(O_3)$ (shaded areas in Fig. 9). It was found that, at the S1 site, when AHC was reduced from 0% to 80%, the corresponding reduction percentage of NO_x should be between 0% and 60% or between 75% and 85% for zero $P(O_3)$ increment. Correspondingly, at the S2 site, the reduction percentages of AHC should be between 0% and 50% more than 95% to avoid an increase in $P(O_3)$. Although a great reduction of $P(O_3)$ would be achieved if over 75% or 95% of NO_x emission was eliminated at S1 and S2, respectively, it may not be practical in the current stage. Therefore, we focused on a reduction range of 0–60% for NO_x. The minimum value of reduction ratio is the ratio of AHC/NO_x reduction when O_3 generation is higher than the baseline scenario under each emission reduction curve, that is, the minimum value of AHC/NO_x corresponding to the intersection of each emission reduction curve and the x-axis. It was determined that the minimum abatement ratio of AHC/NO_x for zero $P(O_3)$ increment should be 1.3 for S1 or 1.6 for S2, the reduction ratios of AHC/NO_x at intersections of the curves and horizontal axis in Fig. 9, and this indicates that more AHC should be reduced at the S2 site. Considering the dominant contributions of xylenes and propene for total RIR and the key sources of xylenes and propene, rougher policies should be primarily applied to paint and solvent usage and the petrochemical industry to diminish O_3 pollution.

5. Conclusions

Online observations of ambient VOCs and trace gases were conducted at 2 sites in Changzhou located in the central YRD region from August to October 2018. Ninety-nine VOC species were detected, including 28 alkanes, 11 alkenes, acetylene, 17 aromatics, 33 halocarbons, 7 OVOCs, and 2 others. The average concentration of VOCs was 39.52 ± 23.14 ppbv. Alkanes, OVOCs, and halocarbons are the major contributors to total VOCs concentration, with a total relative contribution of 74.2%. According to the PMF analysis, traffic-related emissions, and industrial emissions are the main sources of VOCs in Changzhou. Vehicle exhaust was the main anthropogenic source of VOCs, with relative contributions of 38.8%–39.1%, followed by electronic manufacturing#- halocarbons (20.4%–23.0%), paint and solvent usage#-aromatics (14.4%–18.9%), gasoline evaporation (11.1%–7.3%), and petrochemical industry#-ethene & propene (6.4%–5.1%). The relative contributions of individual sources for xylenes and propene were further analyzed. PMF results showed that xylenes were dominantly emitted from paint and solvent usage#-aromatics (60%), electronic manufacturing#-halocarbons (17%), and vehicle exhaust (16%). Different from xylenes, petrochemical industry#-ethene & propene (67%) and vehicle exhaust (30%) were the major sources of propene. Paint and solvent usage, the petrochemical industry, vehicle exhaust, and electronic manufacturing should be given priority to control ambient VOCs and O_3 pollution in the central YRD region.

The sensitivity of O_3 formation to its precursors was investigated using OBM. The RIR values of anthropogenic VOCs (0.86%/% - 0.90%/%), isoprene (0.20%/% - 0.32%/%), and CO (0.11%/% - 0.19%/%) are positive, while the RIR values of NO_x were negative (−1.25%/% - −1.55%/%). As for individual VOC, the RIR values for xylenes and propene are 0.344%/% - 0.356%/% and 0.080%/% - 0.098%/%, accounting for 48.6% and 50.0% of RIR for total anthropogenic VOC species at the S1 and S2 sites, respectively, suggesting the dominant role of AHC in O_3 formation at both sites. The EKMA curve at 2 sites indicated that O_3 formations are in the VOCs-limited regime, which means reducing VOCs may still be an efficient way for the short-term control of O_3. According to the scenario analysis and considering the policy feasibility, the minimum abatement ratio of AHC/NO_x should be no less than 1.3 and 1.6 for S1 and S2, respectively, to prevent the increase of $P(O_3)$. Considering the results above, tougher policies should be applied to paint and solvent usage and the petrochemical industry to reduce the concentrations of xylenes and propene and reduced the local O_3 formation.

CRediT authorship contribution statement

Zhiqiang Liu: Software, Resources, Data curation, Writing – original draft. **Kun Hu:** Methodology, Software, Data curation, Writing – original draft. **Kun Zhang:** Writing – original draft. **Shengnan Zhu:** Writing – original draft. **Ming Wang:** Conceptualization, Methodology, Resources, Writing – review & editing, Supervision. **Li Li:** Conceptualization, Methodology, Resources, Writing – review & editing.

Declaration of competing interest

The authors declare that they have no known competing financial interests or personal relationships that could have appeared to influence the work reported in this paper.

Data availability

Data will be made available on request.

Acknowledgment

This study was financially supported by the National Natural Science Foundation of China (grant nos. 42075144).

Appendix A. Supplementary data

Supplementary data to this article can be found online at https://doi.org/10.1016/j.atmosenv.2023.119755.

References

Cardelino, C.A., Chameides, W.L., 1995. An observation-based model for analyzing ozone precursor relationships in the urban atmosphere. J. Air Waste Manag. Assoc. 45, 161–180. https://doi.org/10.1080/10473289.1995.10467356.

Chen, W.T., Shao, M., Lu, S.H., Wang, M., Zeng, L.M., Yuan, B., Liu, Y., 2014. Understanding primary and secondary sources of ambient carbonyl compounds in Beijing using the PMF model. Atmos. Chem. Phys. 14, 3047–3062. https://doi.org/10.5194/acp-14-3047-2014.

Dorter, M., Odabasi, M., Yenisoy-Karakas, S., 2020. Source apportionment of biogenic and anthropogenic VOCs in Bolu plateau. Sci. Total Environ. 731, 139201 https://doi.org/10.1016/j.scitotenv.2020.139201.

EPA, 2014. EPA Positive Matrix Factorization (PMF) 5.0 Fundamentals and User Guide. United States Environmental Protection Agency, Washington, DC, USA.

Fan, M.Y., Zhang, Y.L., Lin, Y.C., Li, L., Xie, F., Hu, J.L., Mozaffar, A., Cao, F., 2021. Source apportionments of atmospheric volatile organic compounds in Nanjing, China during high ozone pollution season. Chemosphere 263, 128025. https://doi.org/10.1016/j.chemosphere.2020.128025.

He, Z.R., Wang, X.M., Ling, Z.H., Zhao, J., Guo, H., Shao, M., Wang, Z., 2019. Contributions of different anthropogenic volatile organic compound sources to ozone formation at a receptor site in the Pearl River Delta region and its policy implications. Atmos. Chem. Phys. 19, 8801–8816. https://doi.org/10.5194/acp-19-8801-2019.

Lin, H.T., Wang, M., Duan, Y.S., Fu, Q.Y., Ji, W.H., Cui, H.X., Jin, D., Lin, Y.F., Hu, K., 2020. O_3 sensitivity and contributions of different NMHC sources in O_3 formation at urban and suburban sites in Shanghai. Atmosphere 11, 295. https://doi.org/10.3390/atmos11030295.

Liu, Y., Shao, M., Kuster, W.C., Goldan, P.D., Li, X., Lu, S., Gouw, J.A.D., 2009. Source identification of reactive hydrocarbons and oxygenated VOCs in the summertime in Beijing. Environ. Sci. Technol. 43 (1), 75–81. https://doi.org/10.1021/es801716n.

Liu, Y.H., Wang, H.L., Jing, S.A., Gao, Y.Q., Peng, Y.R., Lou, S.R., Cheng, T.T., Tao, S.K., Li, L., Li, Y.J., Huang, D.D., Wang, Q., An, J.Y., 2019. Characteristics and sources of volatile organic compounds (VOCs) in Shanghai during summer: implications of regional transport. Atmos. Environ. 215, 116902 https://doi.org/10.1016/j.atmosenv.2019.116902.

Lu, K.D., Zhang, Y.H., Su, H., Shao, M., Zeng, L.M., Zhong, L.J., Xiang, Y.R., Chang, C.C., Charles, C.K., Andreas, W., 2010. Regional ozone pollution and key controlling factors of photochemical ozone production in Pearl River Delta during summer time. Sci. China Chem. 53 (3), 651–663. https://link.springer.com/article/10.1007/s11426-010-0055-6.

Lu, X.B., Wang, M., Ding, F., Yu, Y.Y., Zhang, Z.H., Hu, K., 2022. Changes of O3-VOCs-NOx sensitivity and VOCs sources at an urban site of nanjing between 2020 and 2021. Environ. sci. 1–18. https://doi.org/10.13227/j.hjkx.202204220.

Lv, Z., Liu, X.Y., Wang, G., Shao, X., Li, Z.Z., Nie, L., Li, G.H., 2021. Sector-based volatile organic compounds emission characteristics from the electronics manufacturing industry in China. Atmos. Pollut. Res. 12, 101097 https://doi.org/10.1016/j.apr.2021.101097.

Man, H.Y., Liu, H., Niu, H., Wang, K., Deng, F.Y., Wang, X.T., Xiao, Q., Hao, J.M., 2020. VOCs evaporative emissions from vehicles in China: species characteristics of different emission processes. Environ. Sci. Ecotechnol. 1, 100002 https://doi.org/10.1016/j.ese.2019.100002.

Mo, Z., Shao, M., Lu, S.H., Qu, H., Zhou, M.Y., Sun, J., Gou, B., 2015. Process-specific emission characteristics of volatile organic compounds (VOCs) from petrochemical facilities in the Yangtze River Delta, China. Sci. Total Environ. 533, 422–431. https://doi.org/10.1016/j.scitotenv.2015.06.089.

Mo, Z.W., Cui, R., Yuan, B., Cai, H.H., McDonald, B.C., Li, M., Zheng, J.Y., Shao, M., 2021. A mass-balance-based emission inventory of non-methane volatile organic compounds (NMVOCs) for solvent use in China. Atmos. Chem. Phys. 21, 13655–13666. https://doi.org/10.5194/acp-21-13655-2021.

Song, C.B., Liu, Y., Sun, L., Zhang, Q.J., Mao, H.J., 2020. Emissions of volatile organic compounds (VOCs) from gasoline and liquified natural gas (LNG)-fueled vehicles in tunnel studies. Atmos. Environ. 234, 117626 https://doi.org/10.1016/j.atmosenv.2020.117626.

Sun, J., Shen, Z.X., Wang, R.N., Li, G.H., Zhang, Y., Zhang, B., He, K., Tang, Z.Y., Xu, H.M., Qu, L.L., Ho, S.S.H., Liu, S.X., Cao, J.J., 2021. A comprehensive study on ozone pollution in a megacity in North China Plain during summertime: observations, source attributions and ozone sensitivity. Environ. Int. 146, 106279 https://doi.org/10.1016/j.envint.2020.106279.

Tan, Z.F., Lu, K.D., Dong, H.B., Hu, M., Li, X., Liu, Y.H., Lu, S.H., Shao, M., Su, R., Wang, H.C., Wu, Y.S., Wahner, A., Zhang, Y.H., 2018. Explicit diagnosis of the local ozone production rate and the ozone-NO_x-VOC sensitivities. Sci. Bull. 63, 1067–1076. https://doi.org/10.1016/j.scib.2018.07.001.

Wang, M., Zeng, L.M., Lu, S.H., Shao, M., Liu, X.L., Yu, X.N., Chen, W.T., Yuan, B., Zhang, Q., Hu, M., Zhang, Z.Y., 2014. Development and validation of a cryogen-free automatic gas chromatograph system (GC-MS/FID) for online measurements of volatile organic compounds. Anal. Methods 6, 9424–9434. https://doi.org/10.1039/C4AY01855A.

Wang, M., Chen, W.T., Zhang, L., Qin, W., Zhang, Y., Zhang, X.Z., Xie, X., 2020a. Ozone pollution characteristics and sensitivity analysis using an observation-based model in Nanjing, Yangtze River Delta Region of China. J. Environ. Sci. (China) 93, 13–22. https://doi.org/10.1016/j.jes.2020.02.027.

Wang, M., Qin, W., Chen, W.T., Zhang, L., Zhang, Y., Zhang, X.Z., Xie, X., 2020b. Seasonal variability of VOCs in Nanjing, Yangtze River delta: implications for emission sources and photochemistry. Atmos. Environ. 223, 117254 https://doi.org/10.1016/j.atmosenv.2019.117254.

Whalley, L.K., Slater, E.J., Woodward-Massey, R., Ye, C., Lee, J.D., Squires, F., Hopkins, J.R., Dunmore, R.E., Shaw, M., Hamilton, J.F., Lewis, A.C., Mehra, A., Worrall, S.D., Bacak, A., Bannan, T.J., Coe, H., Percival, C.J., Ouyang, B., Jones, R.L., Crilley, L.R., Kramer, L.J., Bloss, W.J., Vu, T., Kotthaus, S., Grimmond, S., Sun, Y., Xu, W., Yue, S., Ren, L., Acton, W.J.F., Hewitt, C.N., Wang, X., Fu, P., Heard, D.E., 2021. Evaluating the sensitivity of radical chemistry and ozone formation to ambient VOCs and NO_x in Beijing. Atmos. Chem. Phys. 21, 2125–2147. https://doi.org/10.5194/acp-21-2125-2021.

Xia, S.J., Liu, Q., Zhao, Q.Y., 2018. Emission inventory of anthropogenically sourced VOCs and its contribution to ozone formation in Jiangsu Province. Environ. Sci. 39, 592–599. https://doi.org/10.13227/j.hjkx.201705218 (In Chinese).

Zhang, G., Xu, H.H., Wang, H.L., Xue, L.K., He, J.J., Xu, W.Y., Qi, B., Du, R.G., Liu, C., Li, Z.Y., Gui, K., Jiang, W.T., Liang, L.L., Yan, Y., Meng, X.Y., 2020. Exploring the inconsistent variations in atmospheric primary and secondary pollutants during the 2016 G20 summit in Hangzhou, China: implications from observations and models. Atmos. Chem. Phys. 20, 5391–5403. https://doi.org/10.5194/acp-20-5391-2020.

Zhang, D., He, B., Yuan, M.H., Yu, S.J., Yin, S.S., Zhang, R.Q., 2021. Characteristics, sources and health risks assessment of VOCs in Zhengzhou, China during haze pollution season. J. Environ. Sci. (China) 108, 44–57. https://doi.org/10.1016/j.jes.2021.01.035.

Zhang, K., Huang, L., Li, Q., Huo, J., Duan, Y., Wang, Y., Yaluk, E., Wang, Y., Fu, Q., Li, L., 2021. Explicit modeling of isoprene chemical processing in polluted air masses in suburban areas of the Yangtze River Delta region: radical cycling and formation of ozone and formaldehyde. Atmos. Chem. Phys. 21, 5905–5917. https://doi.org/10.5194/acp-21-5905-2021.

Zhang, K., Liu, Z., Zhang, X., Li, Q., Jensen, A., Tan, W., Huang, L., Wang, Y., de Gouw, J., Li, L., 2022. Insights into the significant increase in ozone during COVID-19 in a typical urban city of China. Atmos. Chem. Phys. 22, 4853–4866. https://doi.org/10.5194/acp-22-4853-2022.

Zhao, Q.Y., Bi, J., Liu, Q., Ling, Z.H., Shen, G.F., Chen, F., Qiao, Y.Z., Li, C.Y., Ma, Z.W., 2020. Sources of volatile organic compounds and policy implications for regional ozone pollution control in an urban location of Nanjing, East China. Atmos. Chem. Phys. 20, 3905–3919. https://doi.org/10.5194/acp-20-3905-2020.